Supporting Information

A Binuclear Cu_A Center Designed in an All α-Helical Protein Scaffold

Evan N. Mirts,[a,b] Sergei A. Dikanov,[c] Anex Jose,[d] Edward I. Solomon,[d,*] and Yi Lu [a,b,*]

[a]Department of Chemistry, [b]Carl R. Woese Institute for Genomic Biology, and [c]Department of Veterinary Clinical Medicine, University of Illinois at Urbana-Champaign, Urbana, Illinois 61801, United States
[d]Department of Chemistry, Stanford University, Stanford, California 94305, United States

Supplemental Methods

XAS of the Cu_ACcP hemoprotein
We separately prepared samples of Cu_AC*c*P with heme bound by titration of hemin into purified apoprotein for the purposes of identifying and compensating for additional copper species that might arise from binding to heme-bound protein contaminants. The heme-bound protein was observed to bind Cu(II) near the heme cofactor, evidenced by a subtle hypsochromic shift in the heme Soret peak position and intensity (Figure S22), and an XAS sample was prepared of Cu(II)-reconstituted Cu_AC*c*P heme-bound protein for comparative modeling. The parameters for the best fit of the EXAFS of this sample are given in Table S3, and the Fourier transform (FT) and fit are shown in Figure S23. One Cys, one His, and two water molecules are included in the first coordination shell. The closer of the two waters is modeled at a distance consistent with a μ-bridging ligand between the heme-Fe and bound Cu(II) ion, a highly unusual binding motif. Of note are the unusually long S_{Cys} and N_{His} bond lengths, each greater than 2.4 Å. Inclusion of heme-Fe and two heme pyrroline N atoms in the second scattering shell dramatically improved the fit (Table S3). The distances of these atoms indicate that the likely position of a bound Cu(II) would lie between the heme Fe and Cys48 with S_{C48}, N_{H52}, and a pair of water molecules comprising the primary coordination sphere.

Crystallization and x-ray diffraction collection conditions for Cu_ACcP hemoprotein
Cu_AC*c*P heme-reconstituted protein was generated from purified apoprotein by addition of ~3 molar equivalents of hemin chloride (10 mM solution, dissolved in 0.1 M potassium hydroxide). Excess hemin was removed by passage through a DEAE Sepharose column. The heme-bound protein was then exhaustively purified through multiple stages of ion exchange chromatography (Mono Q anion exchange column, GE Healthcare) and desalting through a S-200 Sephacryl gel filtration column (GE Healthcare). The purified protein was further exchanged into potassium phosphate buffer (50 mM, pH = 6.0) by passage through a PD-10 gel filtration column (GE Healthcare) and concentrated to 10 mg/mL. Screening drops were set in 24-well hanging drop vapor diffusion trays with 4 µL drops (1:1 ratio of protein and well buffer). Successful drops contained 15-20% PEG 3350 with 50-100 mM potassium thiocyanate with the best crystals obtained from wells containing 100 mM thiocyanate. Diffraction quality crystals always appeared within 24 hours. We collected the x-ray diffraction data of a crystal that was found to diffract to a resolution of 1.6 Å. X-ray diffraction data were collected at SSRL beamline 9-2 equipped with a Dectris Pilatus 6M PAD detector under an Oxford Cryojet cryonic gas stream (100 K) and a wavelength of 0.98 Å. Diffraction image data were processed in HKL2000. The structures were solved and refined in Phenix by single-component molecular replacement against WT C*c*P crystal structures. The heme binding site of the refined structure is shown overlaid with WT C*c*P in Figure S3; the refinement statistics are given in Table S5.

Native electrospray ionization mass spectrometry (ESI-MS)
Mass spectra of Cu-bound Cu_AC*c*P were collected by automated injection of Cu-reconstituted protein through a Thermo Q Exactive ultra high mass range (UHMR) mass spectrometer. Samples were injected with an Advion TriVersa NanoMate chip-based direct infuser. Due to lag time required for sample injection and to minimize sample oxidation, Cu-reconstituted Cu_AC*c*P samples were sealed inside gas chromatography sample vials with a pierceable septum cap immediately following maximum color development and kept on ice until injection. Protein samples were prepared by first exchanging apo-Cu_AC*c*P into ammonium acetate buffer (50 mM, pH = 8.0) and was then reconstituted with Cu by addition of exactly one equivalent of Cu(II) followed immediately by one equivalent of Cu(I) (stabilized in 1 M acetonitrile) to a final protein concentration of 0.05 mM.

Calculation of ^{14}N and ^{1}H HYSCORE parameters

The ^{14}N hyperfine couplings corresponding to cross-peaks $\mathbf{1_N}$ were calculated using the second-order expression for $\nu_{dq\pm}$ [1]

$$A_N = \frac{2\nu_N(\nu_{dq+} + \nu_{dq-})}{8\nu_N - (\nu_{dq+} - \nu_{dq-})}$$

Eq. S1

The estimate based on the maximum value of the double-quantum transitions in orientation-disordered samples used for $\mathbf{1_N}$ and $\mathbf{3_N}$ ($\nu_{dq\pm} = 2[(\nu_N \pm A/2)^2 + K^2(3+\eta^2)]^{1/2}$) is described by the equation

$$A_N = \frac{\nu_{dq+}^2 + \nu_{dq-}^2}{8\nu_N}$$

Eq. S2

where ν_N is the nuclear Zeeman frequency, A_N is the predominantly isotropic hyperfine coupling constant, $K=e^2qQ/4h$ is the quadrupole coupling constant, and η is the asymmetry parameter.[2]

References

(1) Dikanov, S. A.; Tyryshkin, A. M.; Huettermann, J.; Bogumil, R.; Witzel, H. Characterization of Histidine Coordination in VO2+-Substituted D-Xylose Isomerase by Orientationally-Selected Electron Spin-Echo Envelope Modulation Spectroscopy. *J. Am. Chem. Soc.* **1995**, *117* (17), 4976–4986. https://doi.org/10.1021/ja00122a029.

(2) Dikanov, S. A.; Tsvetkov, Yu. D.; Bowman, M. K.; Astashkin, A. V. Parameters of Quadrupole Coupling of 14N Nuclei in Chlorophyll a Cations Determined by the Electron Spin Echo Method. *Chemical Physics Letters* **1982**, *90* (2), 149–153. https://doi.org/10.1016/0009-2614(82)83630-0.

(3) Farrar, J. A.; Neese, F.; Lappalainen, P.; Kroneck, P. M. H.; Saraste, M.; Zumft, W. G.; Thomson, A. J. The Electronic Structure of CuA: A Novel Mixed-Valence Dinuclear Copper Electron-Transfer Center. *J. Am. Chem. Soc.* **1996**, *118* (46), 11501–11514. https://doi.org/10.1021/ja9618715.

(4) Leguto, A. J.; Smith, M. A.; Morgada, M. N.; Zitare, U. A.; Murgida, D. H.; Lancaster, K. M.; Vila, A. J. Dramatic Electronic Perturbations of CuA Centers via Subtle Geometric Changes. *J. Am. Chem. Soc.* **2019**, *141* (3), 1373–1381. https://doi.org/10.1021/jacs.8b12335.

(5) Neese, F.; Zumft, W. G.; Antholine, W. E.; Kroneck, P. M. H. The Purple Mixed-Valence CuA Center in Nitrous-Oxide Reductase: EPR of the Copper-63-, Copper-65-, and Both Copper-65- and [15N]Histidine-Enriched Enzyme and a Molecular Orbital Interpretation. *J. Am. Chem. Soc.* **1996**, *118* (36), 8692–8699. https://doi.org/10.1021/ja960125x.

(6) Lukoyanov, D.; Berry, S. M.; Lu, Y.; Antholine, W. E.; Scholes, C. P. Role of the Coordinating Histidine in Altering the Mixed Valency of CuA: An Electron Nuclear Double Resonance-Electron Paramagnetic Resonance Investigation. *Biophysical Journal* **2002**, *82* (5), 2758–2766. https://doi.org/10.1016/S0006-3495(02)75616-6.

(7) Ross, M. O.; Fisher, O. S.; Morgada, M. N.; Krzyaniak, M. D.; Wasielewski, M. R.; Vila, A. J.; Hoffman, B. M.; Rosenzweig, A. C. Formation and Electronic Structure of an Atypical CuA Site. *J. Am. Chem. Soc.* **2019**, *141* (11), 4678–4686. https://doi.org/10.1021/jacs.8b13610.

(8) Neese, F.; Kappl, R.; Hüttermann, J.; Zumft, W. G.; Kroneck, P. M. H. Probing the Ground State of the Purple Mixed Valence CuA Center in Nitrous Oxide Reductase: A CW ENDOR (X-Band) Study of the 65Cu, 15N-Histidine Labeled Enzyme and Interpretation of Hyperfine Couplings by Molecular Orbital Calculations. *JBIC* **1998**, *3* (1), 53–67. https://doi.org/10.1007/PL00010649.

(9) Epel, B.; Slutter, C. S.; Neese, F.; Kroneck, P. M. H.; Zumft, W. G.; Pecht, I.; Farver, O.; Lu, Y.; Goldfarb, D. Electron-Mediating CuA Centers in Proteins: A Comparative High Field 1H ENDOR Study. *J. Am. Chem. Soc.* **2002**, *124* (27), 8152–8162. https://doi.org/10.1021/ja012514j.

(10) Dikanov, S. A.; Berry, S. M.; Lu, Y. HYSCORE Insights into the Distribution of the Unpaired Spin Density in an Engineered CuA Site in Azurin and Its His120Gly Variant. *Inorg. Chem.* **2019**, *58* (7), 4437–4445. https://doi.org/10.1021/acs.inorgchem.8b03604.
(11) Fernández, C. O.; Cricco, J. A.; Slutter, C. E.; Richards, J. H.; Gray, H. B.; Vila, A. J. Axial Ligand Modulation of the Electronic Structures of Binuclear Copper Sites: Analysis of Paramagnetic 1H NMR Spectra of Met160Gln CuA. *J. Am. Chem. Soc.* **2001**, *123* (47), 11678–11685. https://doi.org/10.1021/ja0162515.
(12) Lappalainen, P.; Watmough, N. J.; Greenwood, C.; Saraste, M. Electron Transfer between Cytochrome c and the Isolated CuA Domain: Identification of Substrate-Binding Residues in Cytochrome c Oxidase. *Biochemistry* **1995**, *34* (17), 5824–5830. https://doi.org/10.1021/bi00017a014.

Table S1. Area of the g_z features of Cu_A spectra with resolved and unresolved hyperfine structure. The low-field half of the g_z feature not overlapping with $g_{x,y}$-region was used for analysis between the initial point of observable spectral intensity increase relative to the base line to the point of maximum intensity of the central component of the 7-line structure. The accuracy of stated values is approx. ±20 MHz.

Species	Width of g_z area (MHz)	A_z (MHz)	Hyperfine Structure	Reference
Cu_AC*c*P	**517**	**45.6**	unresolved	This work
PdII (*P. denitrificans*)	**595**	**86.8**	poorly resolved	3
Tt3L Met160His	**1090**	**-**	unresolved	4
N_2OR	**764**	**120**	resolved	5
Cu_AAz	**1463**	**156.8**	resolved	6
PmoD	**1027**	**141.0**	resolved	7

Table S2. Parameters of the best fit EXAFS simulations for the Cu_A and T2Cu species in Cu_AC*c*P.

		Cu—Cu			Cu—S (Cys)			Cu—N (His)		
Sample	**R Factor**	**N**	**R (Å)**	**σ² (Å²)**	**N**	**R (Å)**	**σ² (Å²)**	**N**	**R (Å)**	**σ² (Å²)**
Cu_ACcP 2eq-Cu Ox	0.0040	1	2.46	0.011	2	2.23	0.018	1	1.93	0.0081
Cu_ACcP 2eq-Cu Red	0.0032	1	2.61	0.0087	2	2.19	0.0036	1	1.91	0.0038
		Cu—O			**Cu—S (Cys)**			**Cu—N (His)**		
Cu_ACcP 0.6eq-Cu	0.0087	1	2.38	0.0075	0.8	2.33	0.0061	1	2.02	0.0052

Table S3. Parameters of the best fit EXAFS simulation for the Cu-bound Cu_AC*c*P heme-bound protein.

			Cu—S (Cys)			Cu—N (His)			Cu—O (H_2O)			Cu—Fe (Heme)			Cu—N (Heme)		
Sample	**χ^2_v**	**R Factor**	**N**	**R (Å)**	**σ² (Å²)**	**N**	**R (Å)**	**σ² (Å²)**	**N**	**R (Å)**	**σ² (Å²)**	**N**	**R (Å)**	**σ² (Å²)**	**N**	**R (Å)**	**σ² (Å²)**
Cu^{2+}-Cu_ACcP-HP	20.56	0.00185	1	2.46	0.011	1	2.48	0.0077	1	1.98	0.010	1	3.29	0.015	1	3.29	0.015
									1	2.92	0.010				1	4.23	0.015

Table S4. Isotropic hyperfine coupling constants (MHz) for Cys C_β protons in Cu_A centers

Species	a_1	a_2	a_3	a_4	Reference
Cu_AC*c*P	8.7	$\|10.8\|^a$			This work
N_2OR	8.6	10.4	11.7	13.3	8
N_2OR	9.1	11.0	12.2	13.8	9
COX	6.8	10.0	12.2	15.4	9
COX[b]	8.1	10.3	11.6	13.3	9
Cu_AAz	9.0		12.5		9
Cu_AAz	~6		~12.5		6
Cu_AAz	$\|7.6\|^a$	10.8	$\|12.8\|^a$		10
Cu_AAz H120G			11.9	$\|13.9\|^a$	10
ba$_3$ oxidase	4.3	8.9	9.5	10.5	11
ba$_3$ oxidase[b]	1.87	9.8		11.4	11
PmoD	4.5			15	7

[a]Linear fit analysis gives two solutions of opposite relative signs for a and T
[b]M160Q variant with Gln replacing Met as an axial ligand

Table S5. XRD statistics for Cu_AC*c*P heme-bound form

Wavelength	0.98 Å
Resolution range	26.89 - 1.60 (1.657 - 1.600)
Space group	P 2_1 2_1 2_1
Unit cell	44.552, 73.547, 101.205; 90, 90, 90
Total reflections	107026
Unique reflections	44632 (4390)
Completeness (%)	1.00
Wilson B-factor	20.54
Reflections used in refinement	44633 (4390)
Reflections used for R-free	2184 (187)
R-work	0.1656 (0.2328)
R-free	0.1854 (0.2687)
Number of non-hydrogen atoms	3002
macromolecules	2365
ligands	43
Protein residues	296
RMS(bonds)	0.006
RMS(angles)	0.78
Ramachandran favored (%)	102
Ramachandran allowed (%)	0.34
Ramachandran outliers (%)	0
Rotamer outliers (%)	0
Clashscore	4.48
Average B-factor	25.45
macromolecules	23.10
ligands	17.86
solvent	35.34

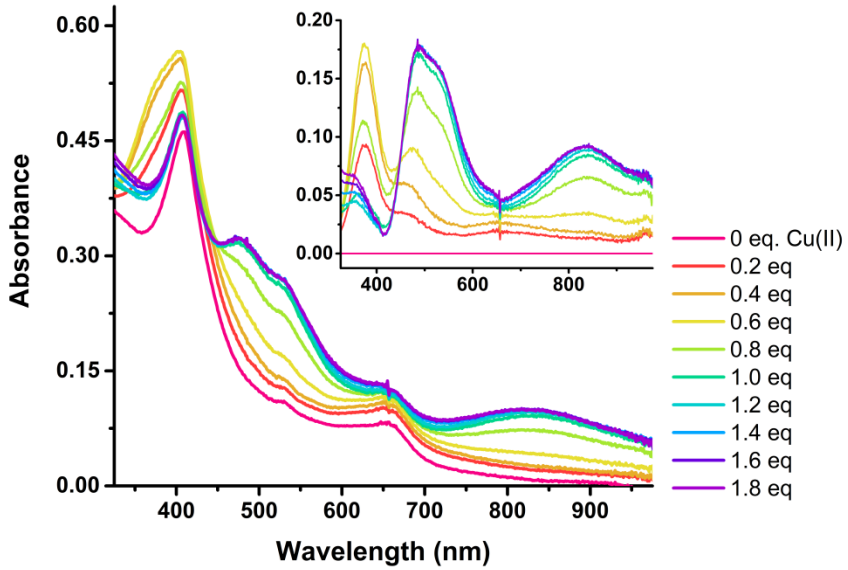

Figure S1. Aerobic titration of 0.1 mM $CuSO_4$ into *apo*-R48C/W51C-C*c*P (difference spectrum, inset).

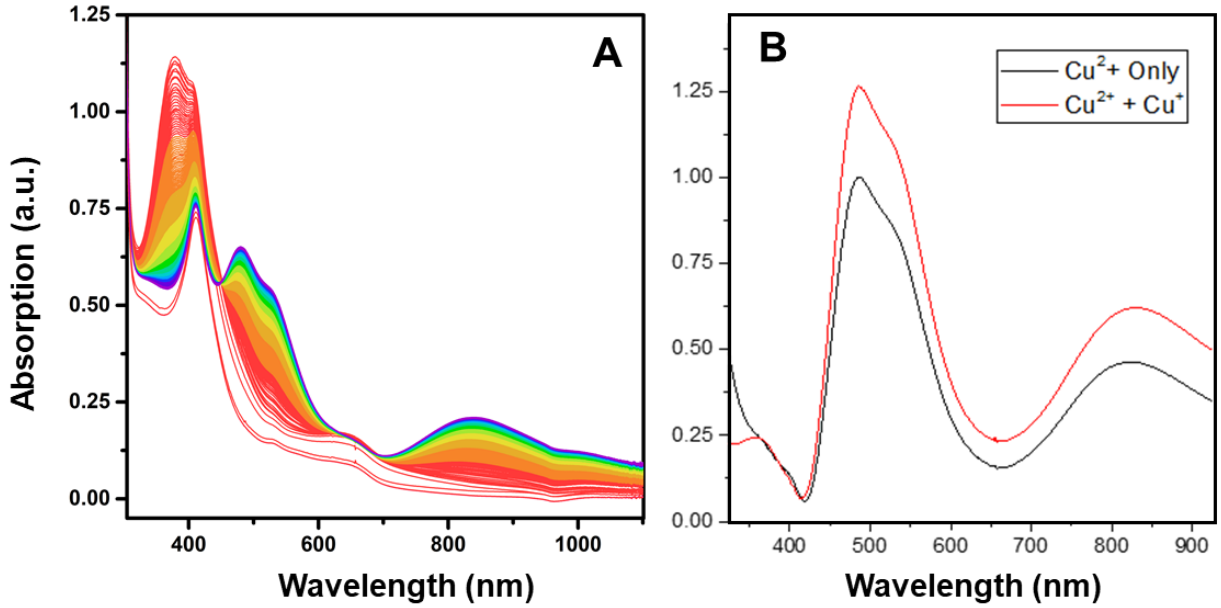

Figure S2. (A) Complete electronic absorption spectra for anaerobic reconstitution of 150 μM Cu_ACcP by addition of 2.5 equivalents of $CuSO_4$ before subtraction of the hemoprotein baseline. Sampling frequency: 0.5 s. (B) Difference spectra obtained by reconstituting apo-Cu_ACcP with either $CuSO_4$ alone (black trace) or by adding alternating sub-equivalents (0.10 eq.) of $CuSO_4$ followed by an equal amount of Cu(I) stabilized in 1 M acetonitrile (red trace). Both spectra are normalized to the maximum absorbance of the Cu(II)-only reconstitution. Yield of the purple species increased by 26% with the mixed Cu(II)/Cu(I) method over Cu(II)-only reconstitution.

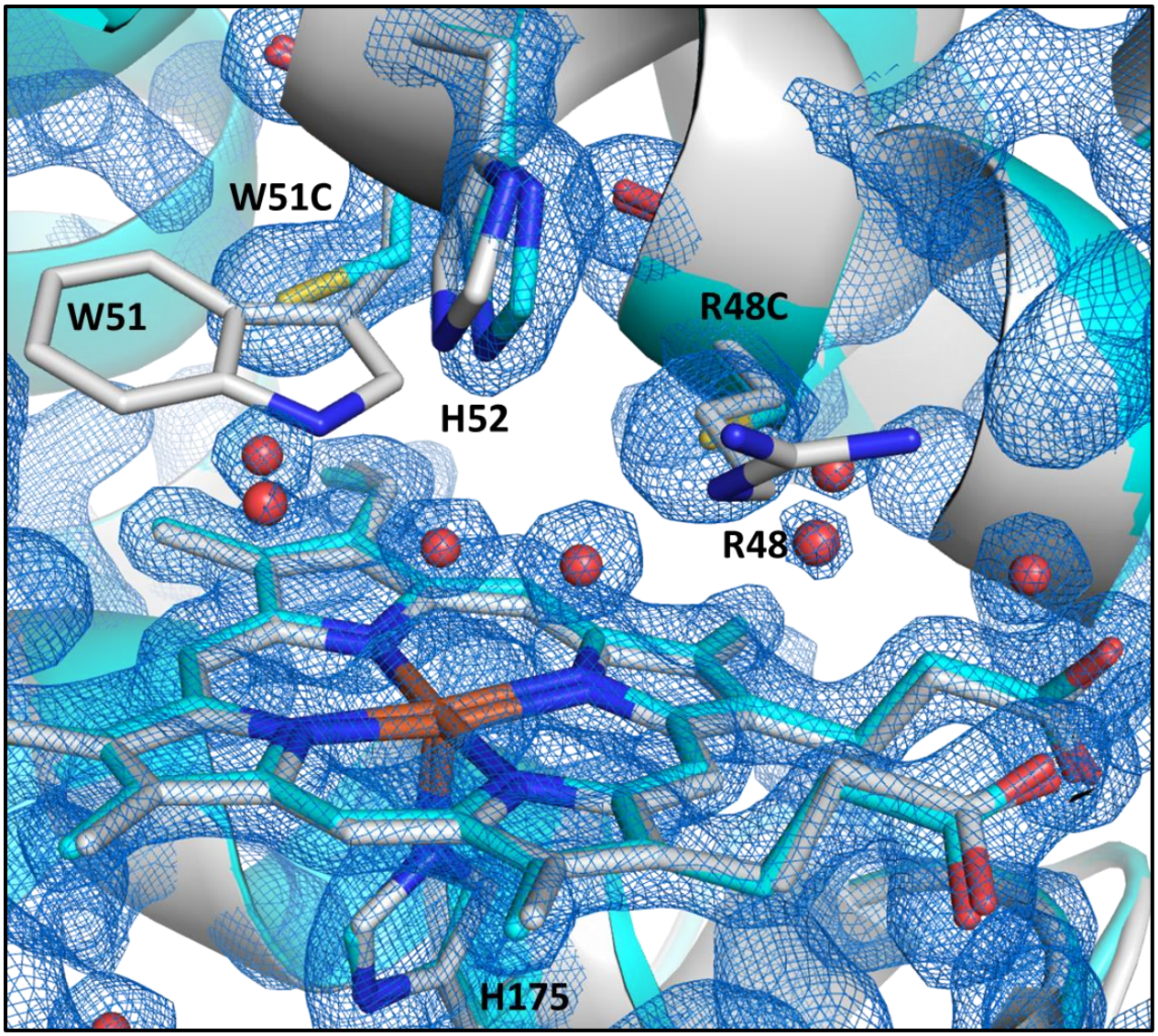

Figure S3. Crystal structure of heme-reconstituted Cu_AC*c*P at refined to 1.60 Å (*cyan*) overlaid with the crystal structure of wild-type C*c*P (*white*, PDB: 2cyp). Water molecules are depicted as red spheres with key residues and the heme cofactors shown in stick representation.

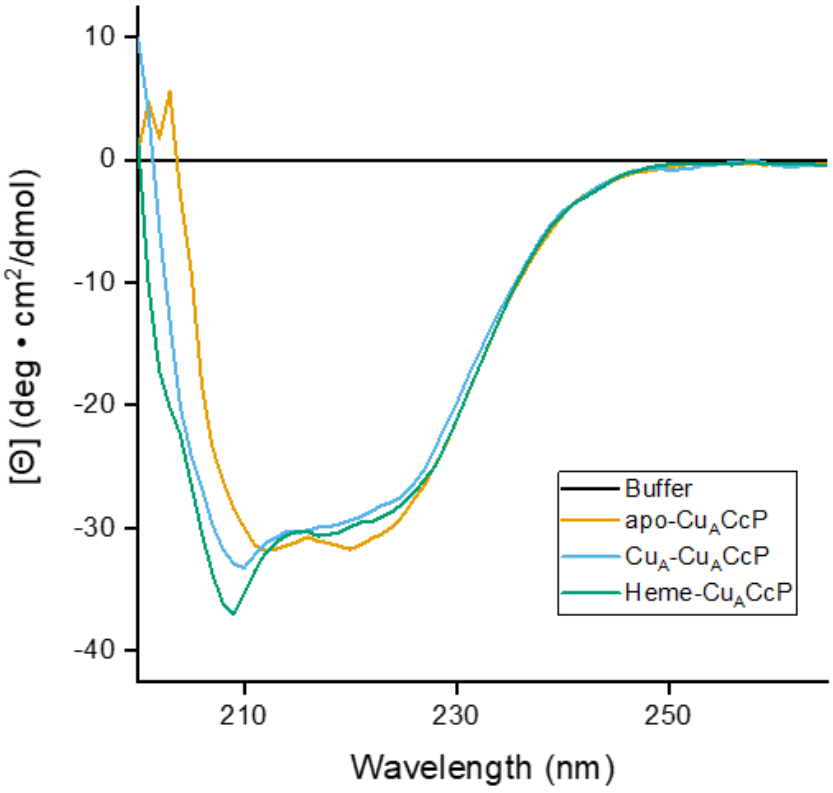

Figure S4. Circular dichroism spectra of apo-Cu$_A$C*c*P, mixed-valent Cu-reconstituted Cu$_A$-Cu$_A$C*c*P, and heme-reconstituted Cu$_A$C*c*P. All protein samples were prepared in metal-free Tris-HCl buffer (50 mM, pH 7.4). Final protein concentrations ranged from 5-10 μM and were adjusted for the optimal instrument detection range. Samples were measured on a Jasco J-715 spectropolarimeter in a cell with a 2 mm pathlength.

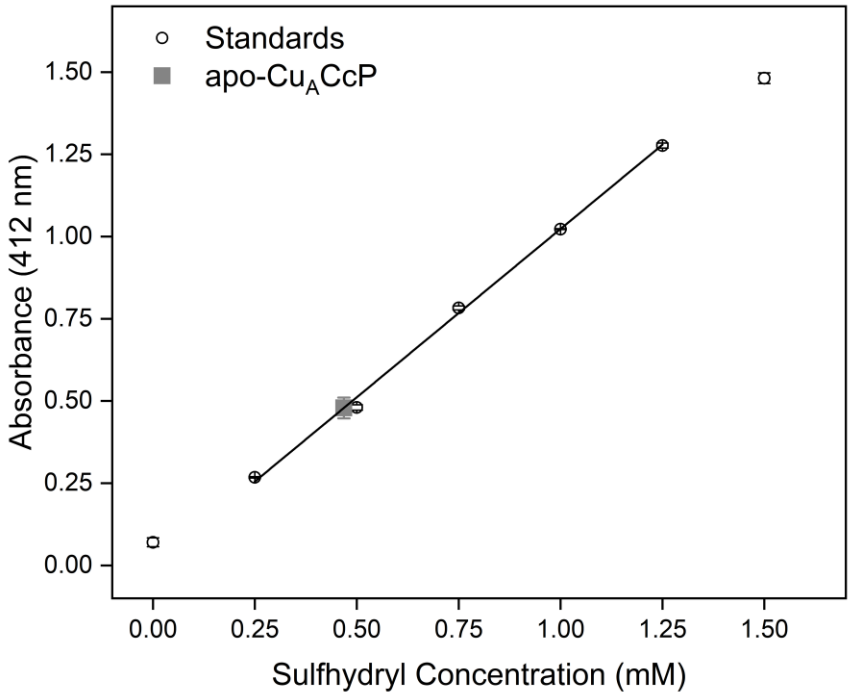

Figure S5. Ellman's test for free sulfhydryl groups. Standards of *L*-cysteine are shown as black circles, and protein samples are shown as gray squares after baseline subtraction. All samples were prepared in 50 mM Tris-HCl buffer (pH 7.4) with 1 mM EDTA reaction buffer. Standards and protein samples were created combining 0.2 mL standard solution with 2.5 mL reaction buffer and adding 50 μL Ellman's reagent (10 mM 5,5-dithio-bis-(2-nitrobenzoic acid); DTNB). Samples were mixed, incubated for 15 min, and then measured at room temperature. All samples were made and measured in triplicate (standard error shown for each point). The apoprotein concentration was 150 μM. The concentration of protein based free Cys was calculated from the linear regression curve fit to the linear region of the standard samples. The concentration of free Cys in the protein samples is 0.469 ±0.032 mM, which is equivalent to 3.12 free Cys per protein monomer.

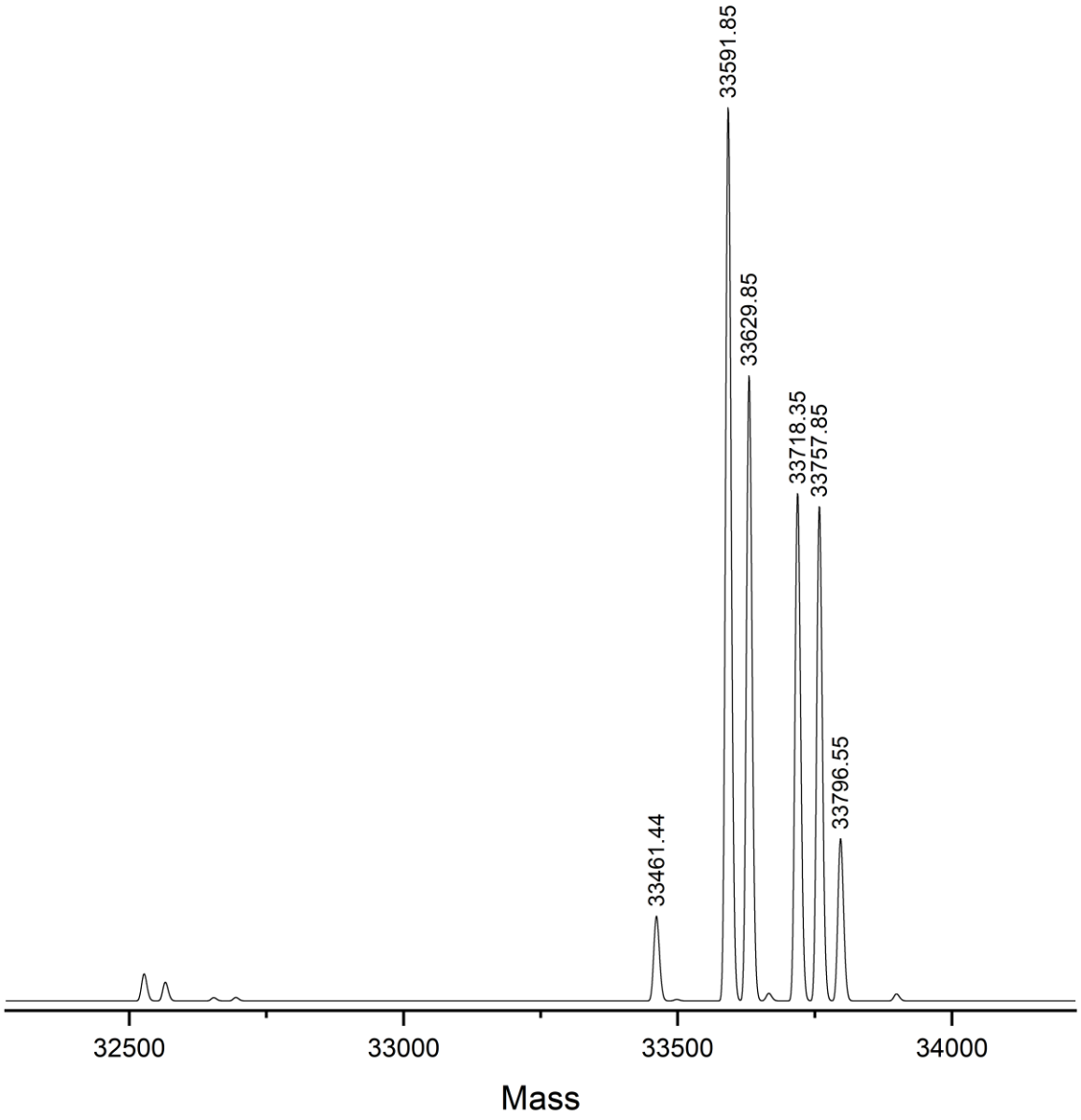

Figure S6. Native ESI-MS of Cu_AC*c*P reconstituted with 2 equivalents of Cu. For each of these peaks, there is a second species of +38.00 and +39.50 Da, respectively, and a third peak (33796.55 Da, +78.20 Da) for the Cu-bound species, all of which likely correspond to protein associated potassium ions (K^+) from the prior protein storage buffer (potassium phosphate) before exchange into ammonium acetate. A minor peak is present at 33461.44 Da (-130.41 Da) that corresponds to a truncation of the C-terminal Leu residue.

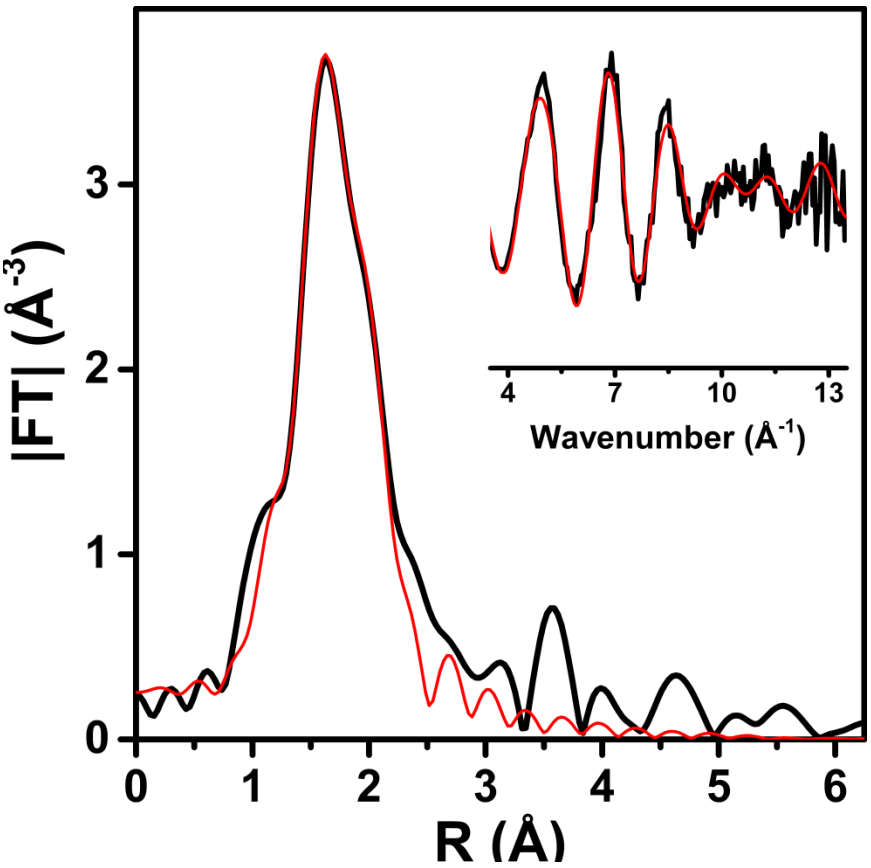

Figure S7. Fourier transform and EXAFS (inset) of the mononuclear T2Cu intermediate prepared with 0.6 equivalents of Cu(II) added to apoprotein. Experimental data are drawn in black, and the best fit simulation is drawn in red.

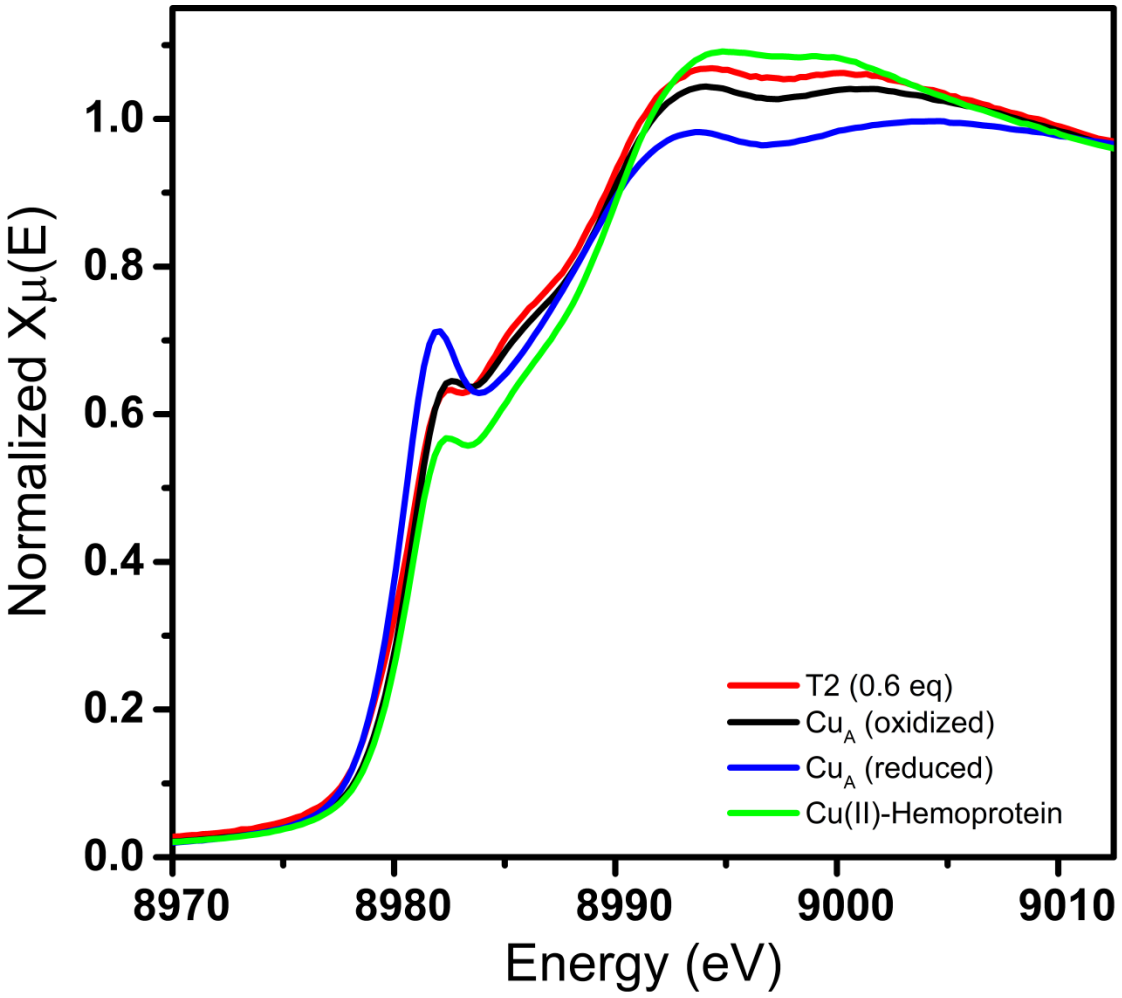

Figure S8. XANES region of the x-ray absorption spectra of all Cu$_A$C*c*P species including the Cu(II)-reconstituted heme-bound protein.

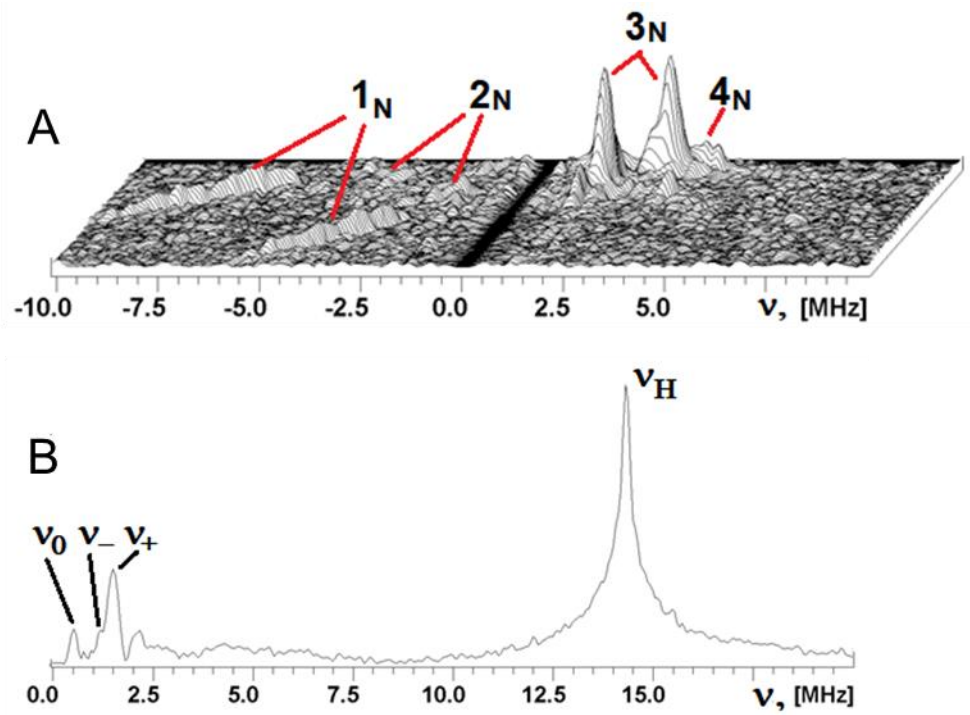

Figure S9. (A) Stacked representation of the ^{14}N HYSCORE spectrum of the Cu_A-like species in Cu_AC_cP. (B) Three-pulse ESSEM spectrum of the Cu_A-like species shows an intense ν_+ = 1.5 MHz line and two lines of lower intensity at ν_0 ~ 0.5 and ν_- = 1.1 MHz which are close to the condition $\nu_+ = \nu_- + \nu_0$ indicating the zero-field nuclear quadrupole frequencies. Observation of this triplet suggests the cancellation condition between hyperfine and external magnetic fields when $A_N \sim 2\nu_N$; i.e., A_N ~2 MHz for the corresponding nitrogen in this experiment. This nitrogen produces also cross-ridges 4_N in HYSCORE spectrum. Microwave frequency = 9.6316 GHz, magnetic field = 336 mT, time between the first and second pulses (τ) = 136 ns.

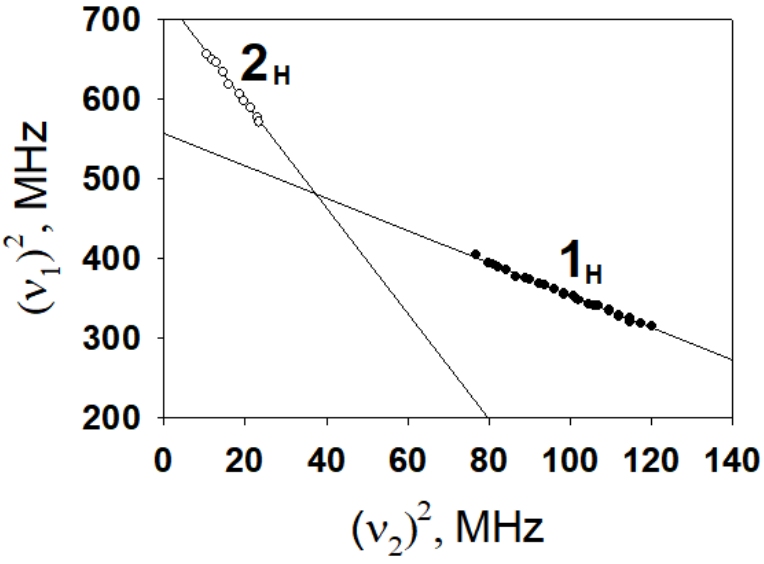

Figure S10. Plots of ^{1}H HYSCORE cross-ridges $\mathbf{1_H}$ and $\mathbf{2_H}$ in the $(\nu_1)^2$ *vs*. $(\nu_2)^2$ coordinate system. The straight lines show the linear fit of plotted data points. The slope *Q* and intercept G for each fit are shown in Table S3. These values were used to obtain two possible solutions for the isotropic (*a*) and anisotropic (*T*) couplings with the same value of $|2a+T|$ and $A_{\perp} = |a - T|$ and $A_{||} = |a+2T|$.

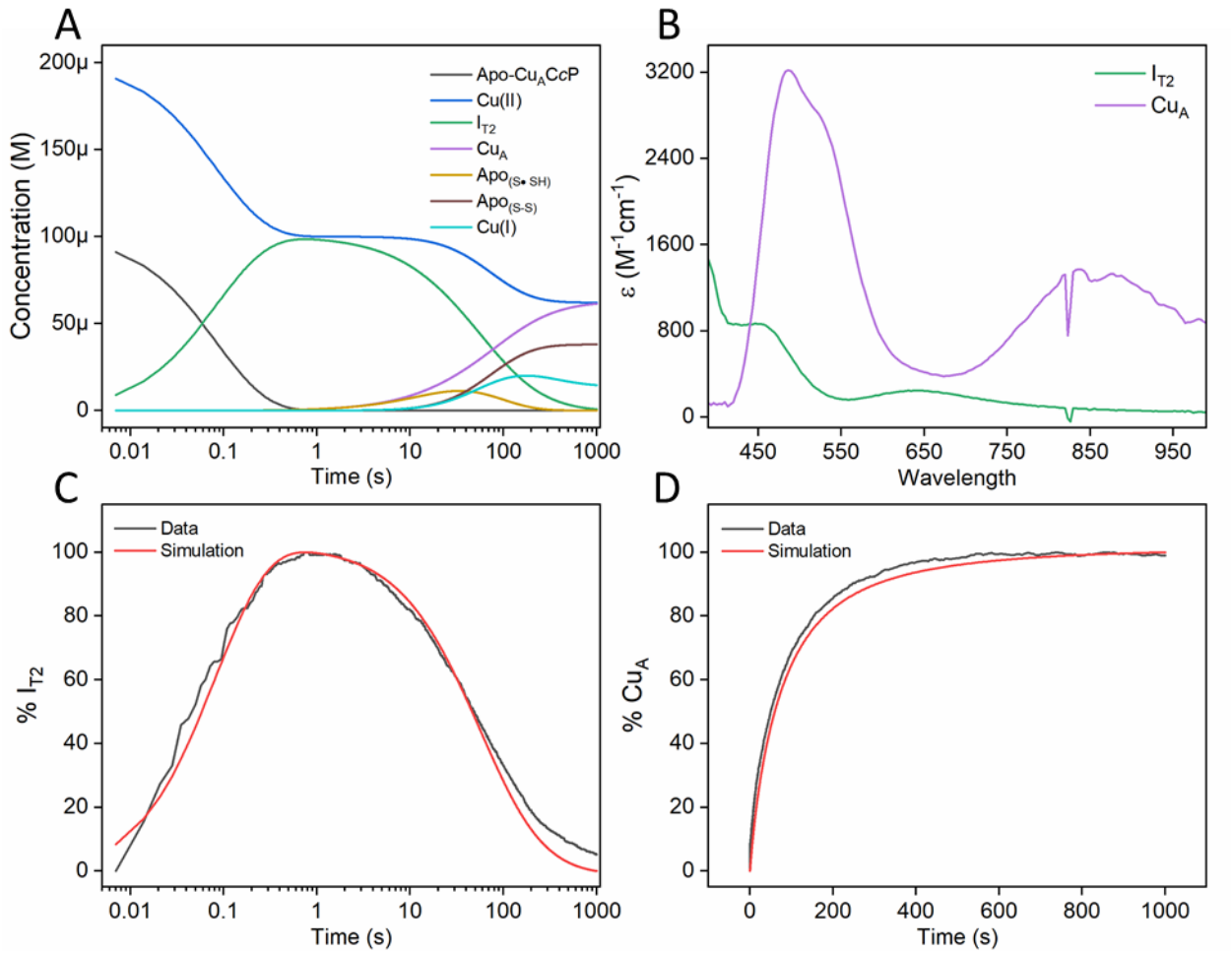

Figure S11. Global spectral analysis of Cu reconstitution of Cu_AC*c*P by a concerted Cu(II) disproportionation model (Model 2 in the main text). (A) kinetic traces of species included in the fitting model. (B) Two chromogenic species were identified as the green T2 intermediate and the binuclear purple Cu species. Due to limitations of the stopped-flow UV spectrometer, only data of wavelengths 360-1000 nm could be obtained. Rate constants for each process are given in Table 4 in the main text. (C, D) Simulated evolution of the T2Cu intermediate (C) and Cu_A (D) species plotted against the experimental data.

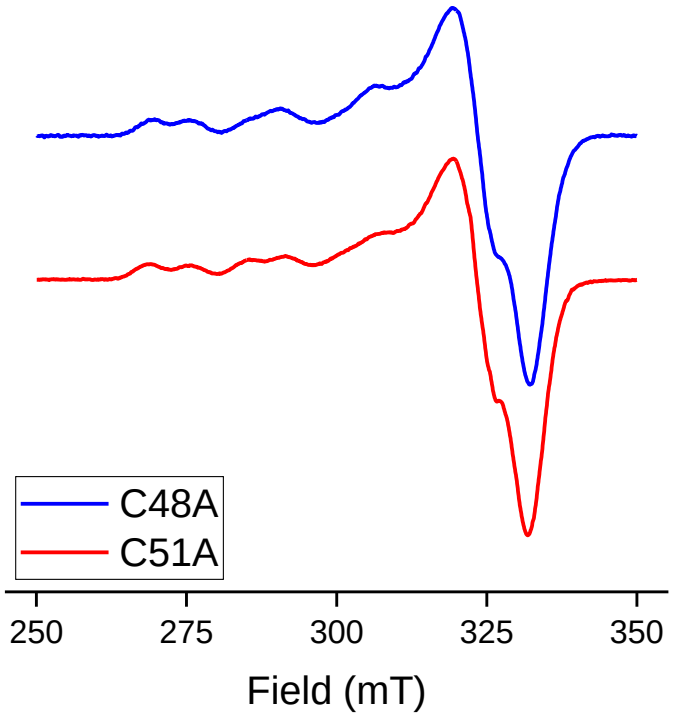

Figure S12. X-band CW EPR spectra of single Cys-to-Ala mutants of Cu_ACcP. Spectra were collected at 77 K and 9.29 GHz with a modulation amplitude of 0.4 mT.

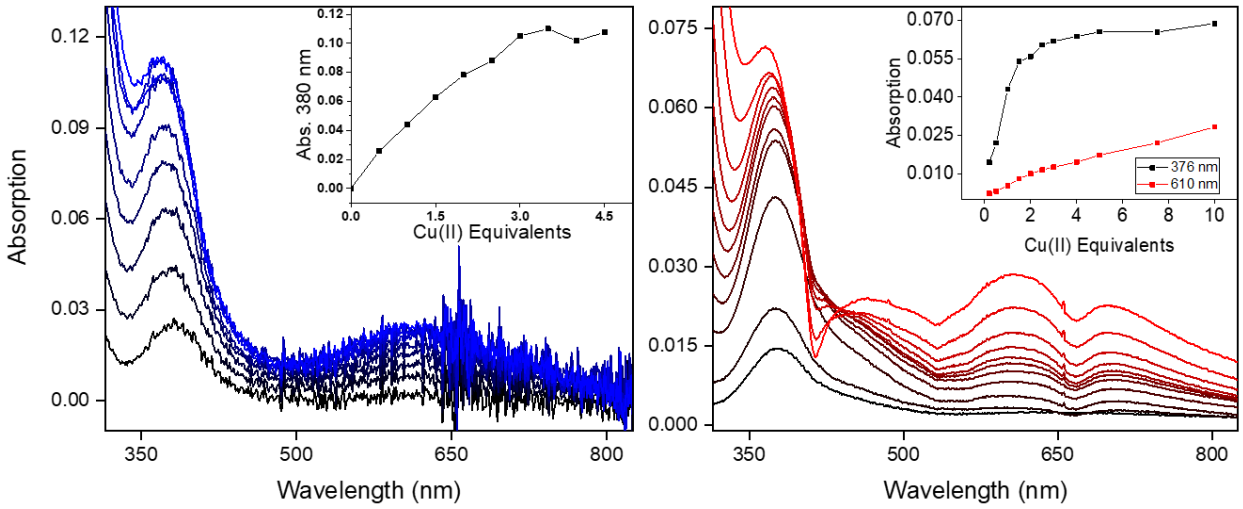

Figure S13. Electronic absorption difference spectra of Cu(II) binding in C48A (*left, blue*) and C51A (*right, red*) single mutants of Cu_ACcP. The concentration of apoprotein in both reconstitutions was 100 μM. T2Cu species form with low absorption maxima for both mutants but require ~4 equivalents of Cu(II) to reach maximum intensity. In W51A, an excess of Cu(II) sulfate (*inset, red trace*) is clearly visible. In C48A the Cu-S CT band maximum is slightly red shifted (380 nm) relative to the T2Cu intermediate in Cu_ACcP while the ~450 nm shoulder is not resolved, and the *d*→*d* band is slightly higher energy at ~620 nm. In C51A, the Cu-S CT band is nearly identical to the T2Cu intermediate with a weakly resolved ~450 nm shoulder, and at low Cu(II) concentrations before excess Cu(II) dominates the spectrum (<2 eq) a weak *d*→*d* band is visible centered at ~660 nm.

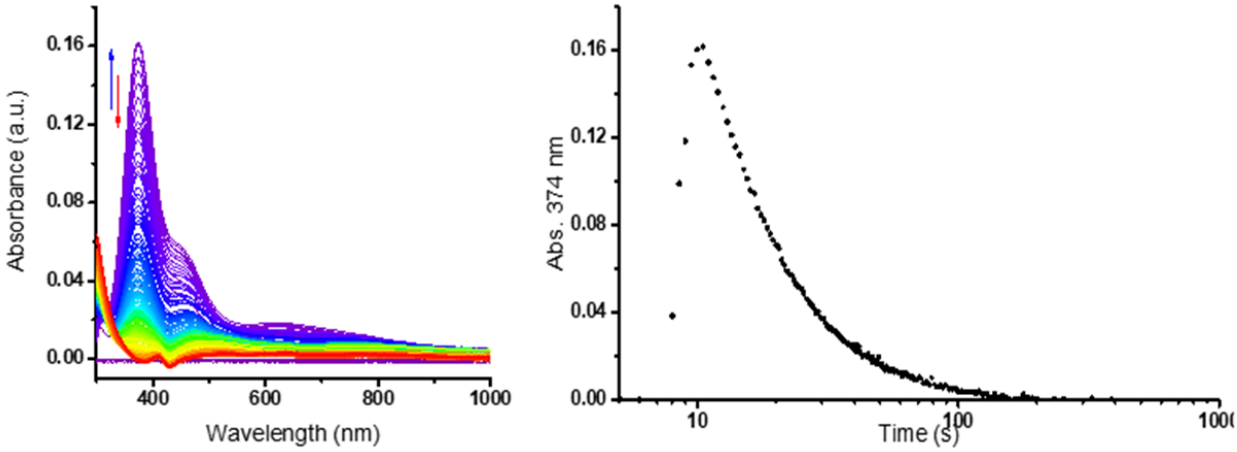

Figure S14. Electronic absorption spectra (Uv-vis) of Cu(II) reconstitution of H52A-Cu$_A$C*c*P. The left spectrum depicts the full species formation and decay cycle after the addition of one molar equivalent of Cu(II), and the right trace shows the formation of the T2Cu species in *ca*. 10s followed by its complete decay in *ca*. 100s. The major absorption bands are nearly identical to the T2Cu intermediate in Cu$_A$ formation in Cu$_A$*c*P. The sampling frequency of these spectra is 0.5 s.

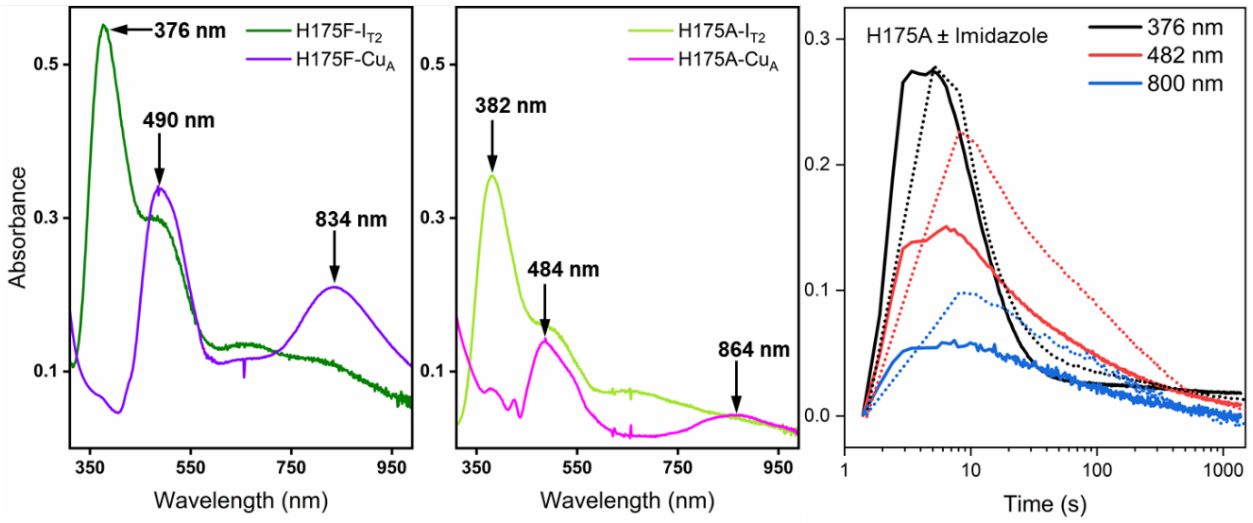

Figure S15. Electronic absorption difference spectra of H175F and H175A mutants of Cu_AC*c*P. Both species form transient T2 intermediates and binuclear Cu species that differ from the native H175 spectra. The H175F mutant (*left*) has a T2 intermediate (*green*) that is nearly identical to the native H175 spectrum. The spectrum of the binuclear species (*violet*) has ~490 nm Cu-S charge transfer peak with less splitting and a blue shifted Cu-Cu $\psi \rightarrow \psi^*$ peak than in H175, suggesting a shorter Cu-Cu distance. The spectra of the H175A mutant (*center*) are similar but with a red-shifted T2 intermediate charge transfer and Cu-Cu peaks relative to H175. Reconstituting the H175A mutant in the presence of 2 equivalents of imidazole (*dotted lines*) produces ~50% more binuclear species with a significantly blue-shifted $\psi \rightarrow \psi^*$ peak (864 nm → 842 nm).

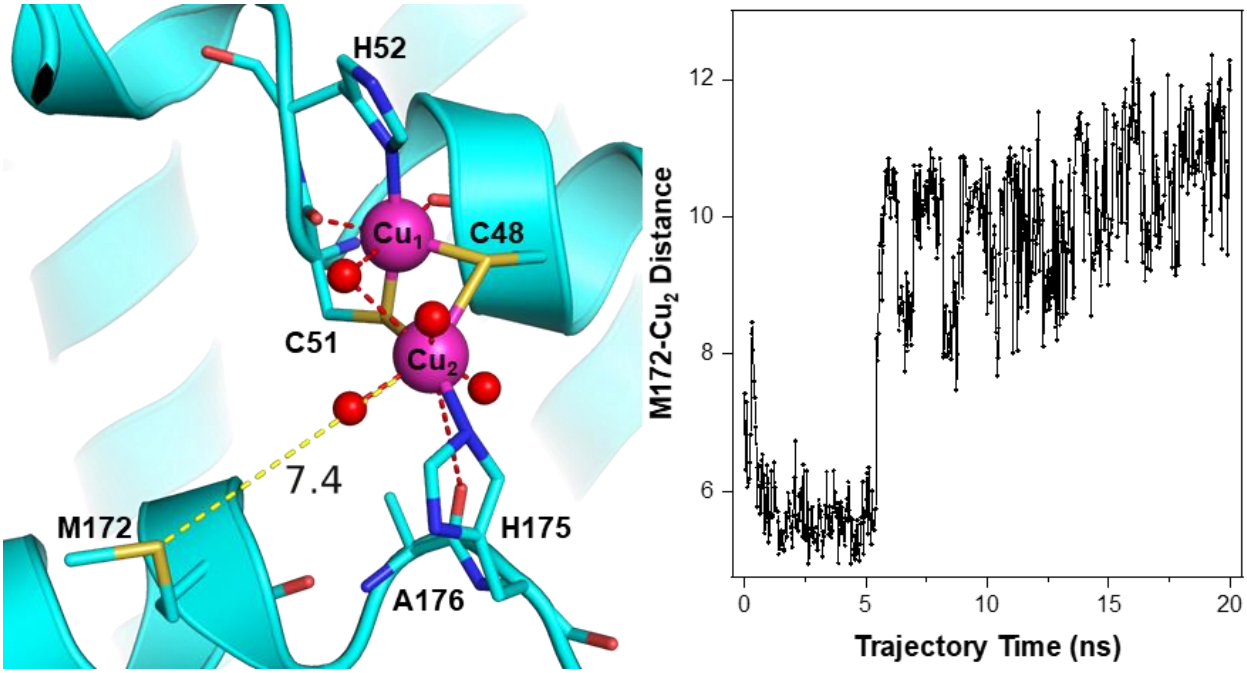

Figure S16. Molecular dynamics (MD) thermal equilibration modeling of the Cu_A binuclear species in Cu_AC*c*P over 20 ns. The initial structure was taken from the solved heme-reconstituted Cu_AC*c*P crystal structure. The distance between the sulfur atom of Met172 and Cu_2 of the binuclear complex is plotted over the equilibration time. Met172 never approaches closer than 5.4 Å whereas over a longer time trajectory the typical separation is ~10 Å. The backbone carbonyl of Ala176 approaches the Cu_2 atom to ~4 Å, but the only available axial ligands to Cu_2 within a reasonable bond distance are water molecules (red spheres).

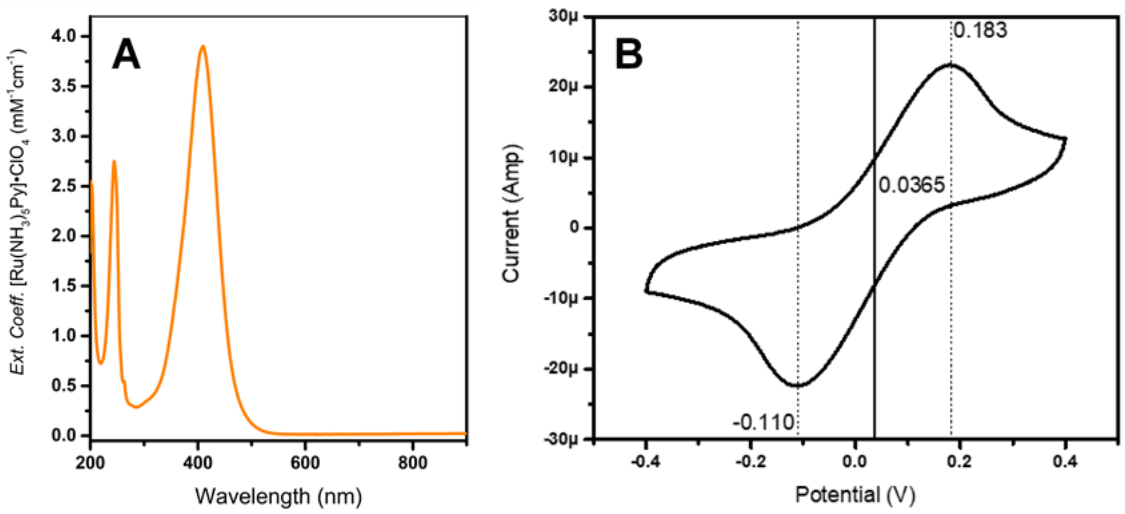

Figure S17. (A) Electronic absorption spectrum of the final product in $[Ru(NH_3)_5Py]\cdot ClO_4$ synthesis. (B) Voltammogram of the complex measured under the same conditions as the redox titration Ag/AgCl reference electrode calibrated to NHE (-307 mV).

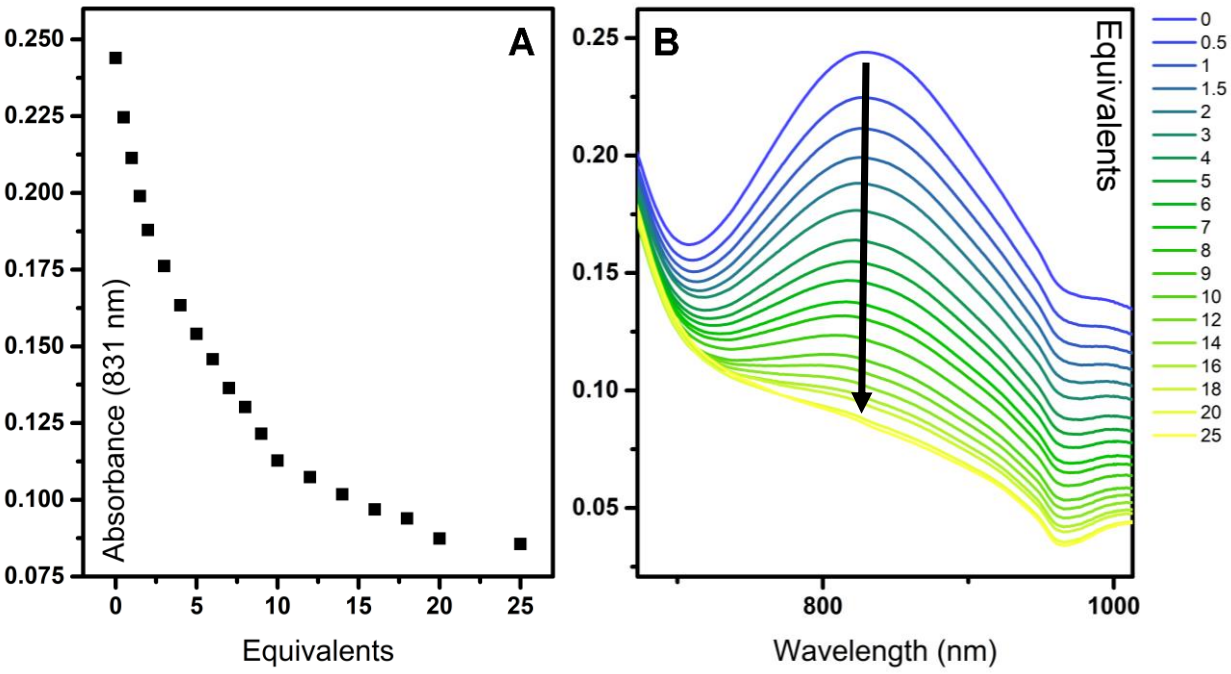

Figure S18. (A) Scatter plot of the absorbance of the Cu_ACcP sample at 831 nm during redox titration by $[Ru(NH_3)_5Py]\cdot ClO_4$ complex. (B) Electronic absorption spectrum of the titration in the NIR region. The broad peak at 831 nm is unimpacted by the absorption from the Ru^{2+} complex and was therefore chosen as a point of reference.

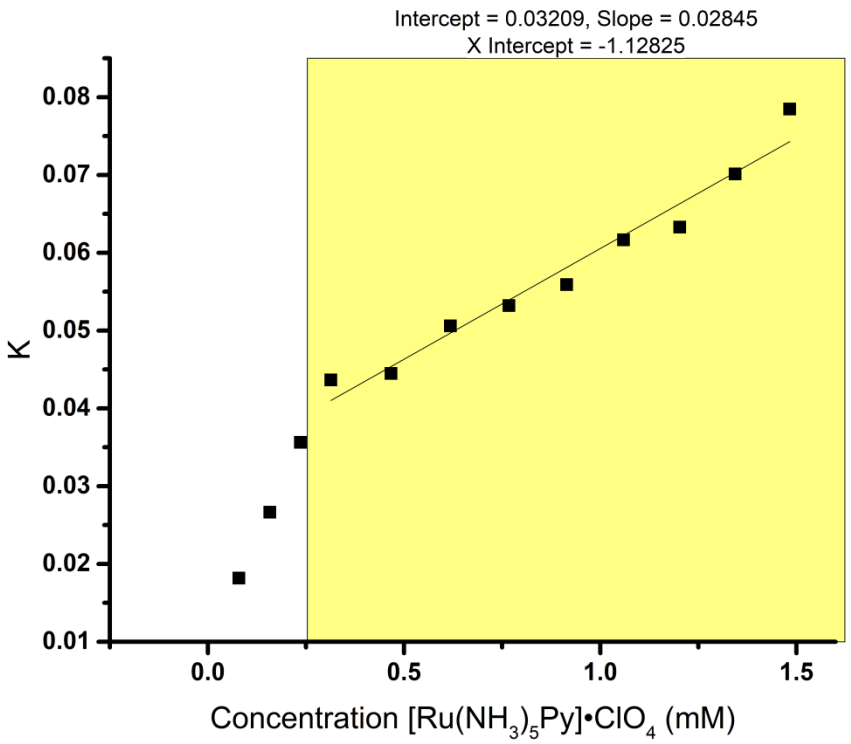

Figure S19. Scatter plot of *K* as calculated as a result of Cu_ACcP redox titration by Ru^{2+} complex. The value of *K* used to determine the reduction potential of Cu_ACcP copper center was the value for a linear fit of the linear region of *K* vs conc. $[Ru]^{2+}$ complex extrapolated to zero.

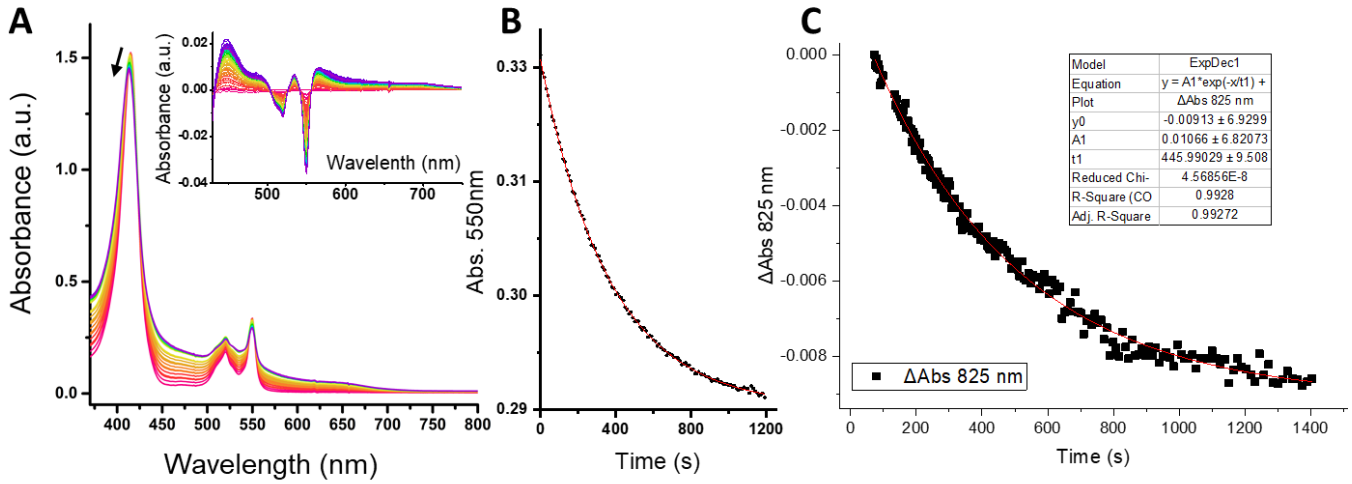

Figure S20. Electron Transfer from Fe(II)-cyt.*c* to mixed valent Cu_AC*c*P. (A) Addition of up to 5 molar equivalents of Cu_AC*c*P causes the Soret peak of a solution (10 μM) of ferrous bovine heart cytochrome *c* type-IV (cyt.*c*) to decrease in intensity and shift from 415 nm toward the 409 nm ferric peak (*black arrow*). The intensity at 550 nm also decreases relative to baseline absorption and is replaced by ferric features in the visible spectrum (inset, difference spectrum). (B) Time trace of the total absorbance at 550 nm upon addition of 5 molar equivalents of Cu_AC*c*P (black points) fit with a single exponential equation (red line). We calculated the first order rate constant to be $k = 2.74 \times 10^{-3}$ s^{-1} ($\pm 1.5 \times 10^{-5}$ s^{-1}). (C) Electron transfer from Fe(II) cyt.*c* to mixed valent Cu_AC*c*P by monitoring the decrease in absorption of the ~800 nm feature. Five equivalents of reduced cytochrome *c* were added to 1.5 mL of 50 μM mixed valent Cu_ACcP. In the difference spectra, the ideal wavelength was 825 nm for monitoring the change in this feature to minimize background effects from excess cyt.*c*. From this experiment, we also found the ET reaction to be first order, and we calculated a rate constant $k = 2.24 \times 10^{-3}$ ($\pm 4.8 \times 10^{-5}$) s^{-1}, which is quite similar to the rate we found by monitoring the change in cyt.*c* oxidation at 550 nm. Relying on previous studies of ET rates in native Cu_A that showed a lower noise in the 550 nm absorption data,[12] the data from monitoring cyt.*c* oxidation are likely to be more reliable. All measurements were conducted in a stirred quartz cuvette maintained at 25°C by a circulating water bath. Red lines are the first order exponential fits.

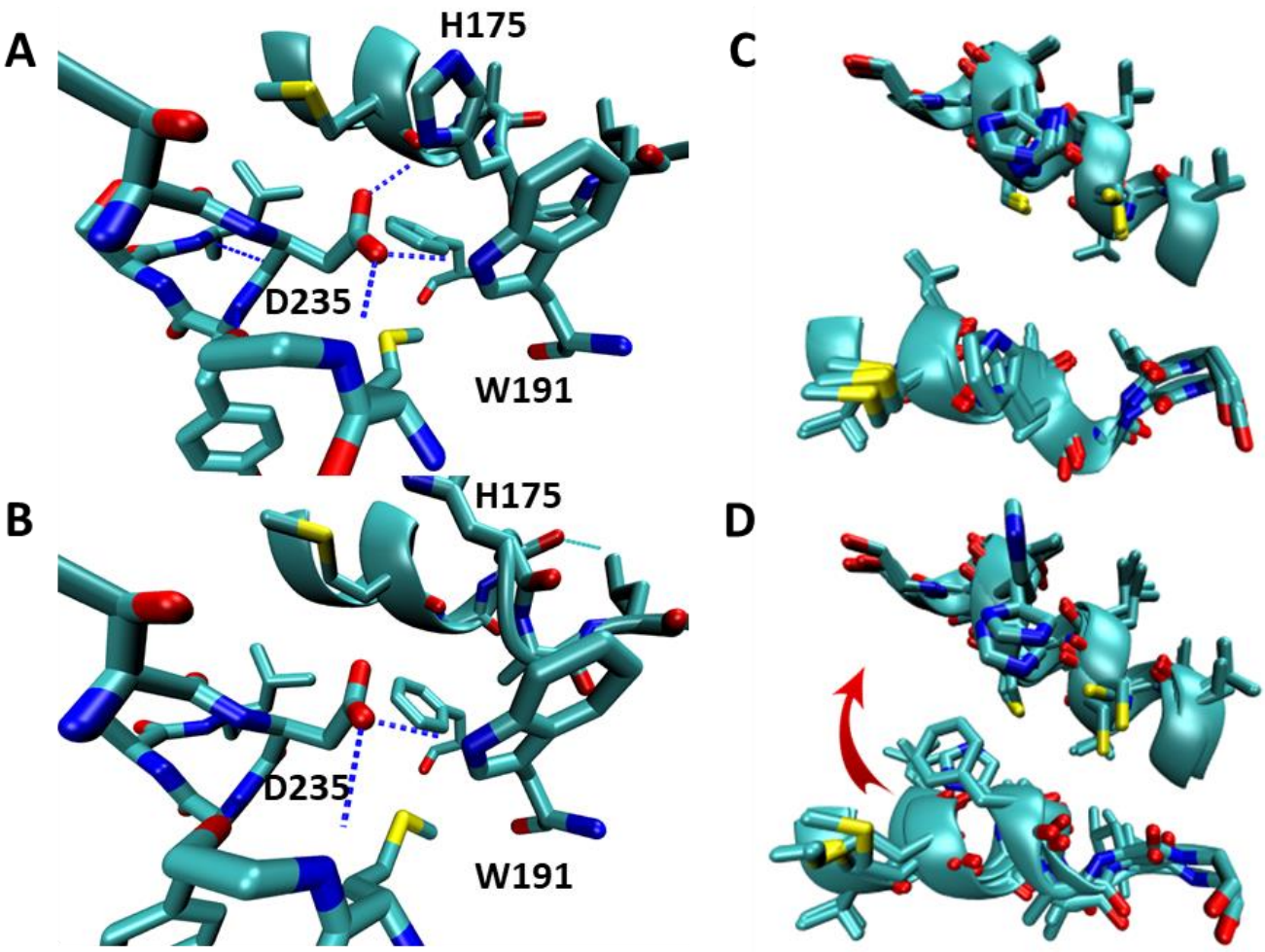

Figure S21. Results of MD simulations for His/Ala/Phe175 apo-Cu_AC*c*P. Panels A (initial energy minimized structure) and B (after 5 ns of thermal equilibration) show the maintenance of the hydrogen bonding network about Asp235 for native His175 even after His175 migrates away; blue dashes indicate stable hydrogen bonds. Panels C (initial energy minimized structure) and D (after 5 ns) show the migration of both mutant and native residues on the helix bearing His175, demonstrating that the helix relaxes regardless of the identity of residue 175, with all mutants aligning similarly after ~5 ns; the red arrow indicates the movement of residue 175.

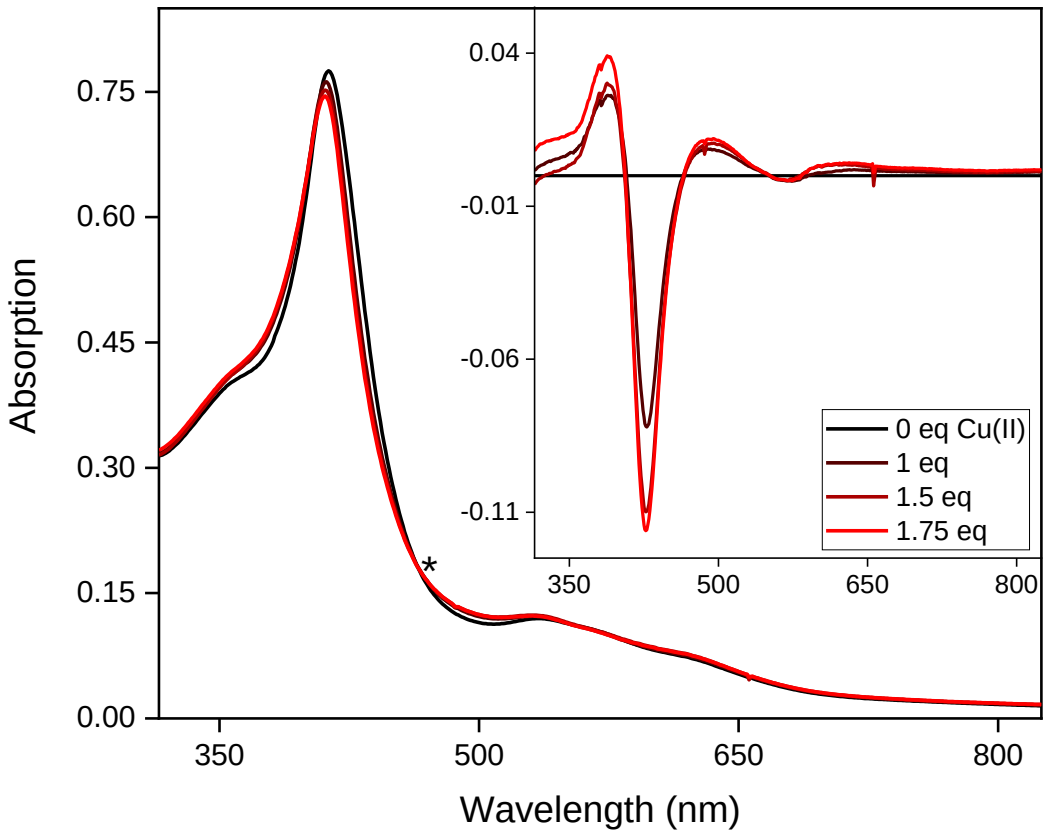

Figure S22. Titration of Cu(II) into Cu_ACcP reconstituted with heme: UV-visible absorption spectra with the difference spectra given as an inset. The hemoprotein was found to bind Cu(II), causing a small shift in the Soret peak maximum from 413 nm to 411 nm. The effect saturated at ~2 equivalents of Cu(II). Isosbestic points are present at multiple points in the spectra with the most obvious occurring at 406 nm and 465 nm (*asterisk*).

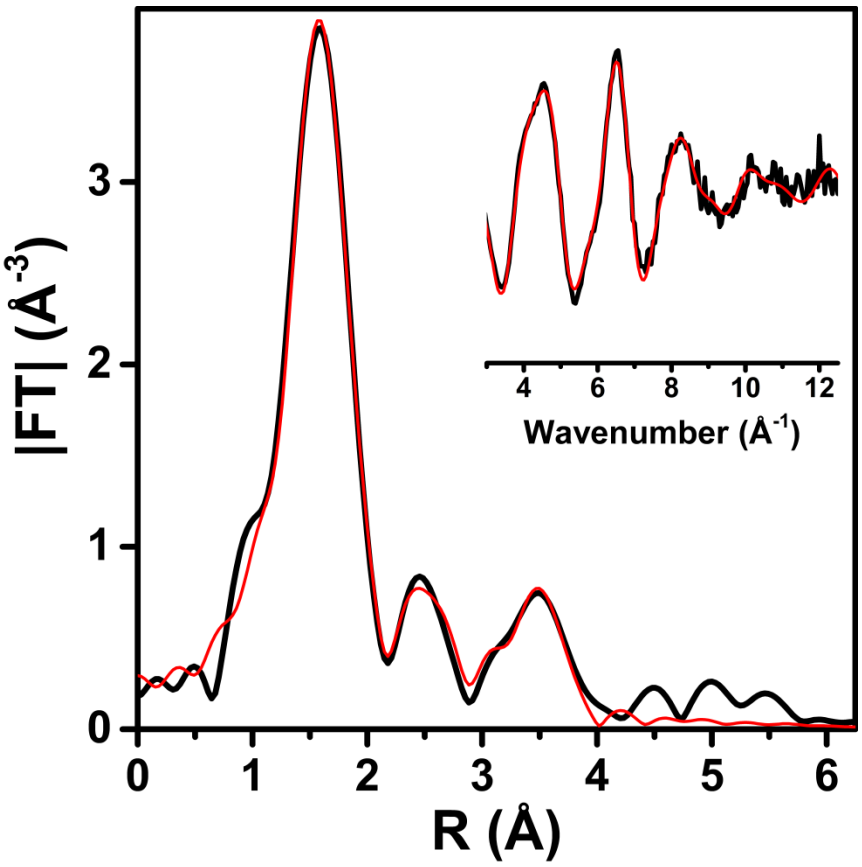

Figure S23. Fourier transform and EXAFS (inset) of Cu(II)-reconstituted into the heme-bound form of Cu_ACcP. Experimental data are drawn in black, and the best fit simulation are in red. Fit parameters are given in Table S3.